Polymer 202 (2020) 122680

Contents lists available at ScienceDirect

Polymer

journal homepage: http://www.elsevier.com/locate/polymer

On the nucleation of polylactide by melt-soluble oxalamide based organic compounds

Manta Roy [a], Maksim Zhelezniakov [a], Gijs W. de Kort [a], Laurence G.D. Hawke [a], Nils Leoné [a], Sanjay Rastogi [a], Carolus H.R.M. Wilsens [a,b,*]

[a] Aachen-Maastricht Institute for Biobased Materials (AMIBM), Faculty of Science and Engineering, Maastricht University, Urmonderbaan 22, 6167, RD, Geleen, the Netherlands

[b] SABIC Technology & Innovation, STC Geleen, Urmonderbaan 22, Geleen, The Netherlands

ARTICLE INFO

Keywords:
Bisoxalamide organic compounds
Crystallization
Nucleation
Polylactide

ABSTRACT

In this work, a series of oxalamide based organic compounds (OBOC) are synthesized and their capability to enhance the nucleation of polylactide is reported. The OBOCs are soluble in the polylactide melt and crystallize upon cooling, providing surface for heterogeneous nucleation to the polylactide matrix. One interesting observation is that the nucleation efficiency of the OBOCs increases at high cooling rates, making the use of OBOCs as a nucleating agent attractive for industrial processing conditions. The paper addresses the mechanism involved in the cooling rate dependence on the nucleation efficiency of the OBOC: The nucleation efficiency of polylactide is significantly enhanced in the presence of OBOC crystals, as a transcrystalline PLA morphology grows from the OBOC crystal surface (at relatively low supercooling from the equilibrium melting temperature of PLA). However, such crystallization of PLA occurs only when the OBOC crystals are formed at or below 145 °C while cooling at 10 °C/min. In contrast, when the OBOC crystals are formed above 145 °C (*i.e.* from a lower supersaturated state), the OBOC crystals display a significantly reduced capability for PLA nucleation. These findings override the possibility of both epitaxy and soft-epitaxy as a plausible nucleation mechanism. Supported by polarized optical microscopy, differential scanning calorimetry, plate-plate rheology and molecular modelling we evaluate the possibility of nucleation resulting from local stresses imposed on the polylactide melt invoking stress-enhanced nucleation. The imposed local shear rates, facilitated by the rapid growth of the OBOC crystals, are found high enough to facilitate contour orientation of the high molecular weight PLA chains next to the growing OBOC crystals, confirming the possibility for stress-enhanced nucleation. In addition, we identify surface roughness of OBOC crystals as a second parameter that influences the PLA nucleation process; the OBOC crystallization at high supersaturation is expected to yield smaller/defected OBOC crystals, which are presumed to provide high surface area and surface roughness. In contrast, when the OBOC crystals are grown at lowered supersaturation (>150 °C), they are bound to anneal during crystallization, providing a smoother surface and lower surface area – retrospectively exhibiting a decreased capability to promote the PLA nucleation, irrespective of the PLA supercooling. Interestingly, both the surface roughness of OBOC crystals and the local stresses they impose on the PLA melt increase when the OBOC crystal growth proceeds from a highly supersaturated state, providing an explanation to the cause of the favored crystallization of PLA at the high cooling rates in the presence of the chosen OBOCs.

1. Introduction

Polylactide (PLA) has attracted considerable attention in the recent years, resulting from its renewable origin [1–4], biocompatibility [5,6] and biodegradability [7]. Nevertheless, though PLA is considered a promising renewable polymer, it suffers from brittleness, low impact resistance, and poor long-term behavior due to its pronounced creep [8,9]. The latter is mostly the result of the low crystallinity of PLA after processing, resulting from its slow nucleation and crystallization kinetics [10]. Though the supercooling provides the driving force for the

* Corresponding author. Aachen-Maastricht Institute for Biobased Materials (AMIBM), Faculty of Science and Engineering, Maastricht University, Urmonderbaan 22, 6167, RD, Geleen, the Netherlands.
E-mail address: karel.wilsens@sabic.com (C.H.R.M. Wilsens).

https://doi.org/10.1016/j.polymer.2020.122680
Received 14 January 2020; Received in revised form 19 May 2020; Accepted 30 May 2020
Available online 10 June 2020

homogenous nucleation and crystallization process of PLA, the nucleation process can be enhanced by the addition of a nucleation agent [11–13] (NA), potentially addressing the aforementioned limits in mechanical performance.

Numerous additives, for example, calcium carbonate [14], cellulose [15], clay [16], talc [17], functionalized lignin [18], hydrazides [19,20], amino-acids [21], and oxalamides [22] have been reported to enhance the nucleation rate of the PLA melt. When using inorganic compounds, irrespective of the nucleation mode, the observed nucleating efficiency is generally limited by the (in)homogeneity of the dispersion of the filler in the polymer matrix. In this respect, the use of melt-soluble organic nucleating agents are preferred. These organic molecules are designed to dissolve in the polymer melt and crystallize on cooling – prior to crystallization of the polymer melt. It is to be realized that on decreasing the temperature of the polymer/NA solution, the solubility of the NA decreases until a supersaturated state is achieved that promotes nucleation and crystallization of the NA; a process that is dependent on both the temperature and the NA concentration in the polymer melt. Crystallization of the NA from such a supersaturated state effectively yields a homogenous dispersion of NA crystals throughout the polymer matrix. In turn, the overall nucleating efficiency of the polymer matrix is determined by the geometry and the surface-to-volume ratio of the NA crystals, which in turn is dependent on the thermal history of the sample, and hence the supersaturation of the system prior to the NA crystallization.

An example of melt-soluble nucleating agents are oxalamide based organic compounds (OBOC). Generally, two oxalamide moieties are connected through a bridging spacer, which is varied to control the OBOC melting temperature. Secondly, the end-groups of the OBOC are selected such that they promote miscibility with the polymer matrix of choice. When designed correctly and used in sufficient concentration, the side groups stimulate dissolution in the polymer matrix at elevated temperatures, while the hydrogen bonding between the oxalamide moieties provides the driving force for crystallization from the polymer melt upon cooling [23,24]. Indeed, this approach proved successful in designing melt-soluble nucleating agents for several polymers including polyhydroxyalkanoates [23], isotactic polypropylene [24,25], polylactide [22,26], and poly(butylene-adipate) [27,28]. Though this generic approach in designing nucleating agents for thermoplastic polymers is promising, the mode of nucleation is not clear; Given that multiple OBOCs can effectively enhance the nucleation efficiency of different polymers, we consider nucleation by epitaxial matching as general OBOC nucleation mechanism unlikely. Therefore, the purpose of this work is to evaluate various nucleation mechanisms and identify the critical parameters responsible for the enhancement of the PLA nucleation process in the presence of OBOCs.

2. Experimental section

2.1. Material preparation and blending process

Five different OBOCs have been synthesized according to the procedure described in earlier work, Scheme 1 [23]. As an example, the synthesis of diethyl 5,6,11,12-tetraoxo-4,7,10,13-tetraazahexadecane-1,16-dioate, abbreviated as OXA2, is briefly recalled; 1,2-diaminoethane was dropwise added to a 10-fold excess of diethyloxalate in THF and the mixture was allowed to stir for 24 h at room temperature. The intermediate product, diethyl 2,2'-(ethane-1,2-diylbis (azanediyl))bis (2-oxoacetate), precipitated during the reaction and was obtained as a white powder after filtration and washing three times with diethyl ether. Next, diethyl 2,2'-(ethane-1,2-diylbis (azanediyl))bis(2-oxoacetate) was dissolved in chloroform together and a double molar excess of β-alanine ethyl ester hydrochloride and triethyl amine. The product, OXA2, precipitated over time during refluxing for 48 h and was obtained as a white powder after filtration and washing three times with chloroform. Details on the synthesis, analysis and thermal behavior of the purified

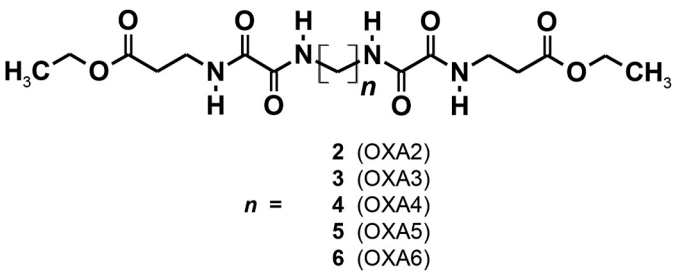

Scheme 1. Chemical structures of the five OBOCs used in this study. The OBOCs are abbreviated based on the number of methylene groups in-between the oxalamide units; For example, the OBOC based on 1,2-ethanediamine, having two methylene groups between the oxalamide groups, is named OXA2.

OBOC materials are provided in the Supporting Information.

The synthesized OBOCs are dried overnight at 60 °C *in vacuo* together with the PLA (Corbion L130 grade, <1% D-enantiomer). Master batches of 10 wt% OBOC in PLA are prepared through extrusion for 3 min in a DSM Xplore twin-screw extruder (5 ml barrel size) at 180 °C and at 100 RPM. Next, the master-batches are diluted with PLA to obtain samples of 0.5, 1.0, 1.5, and 2.0 wt% OBOC. After extrusion, the samples are cooled to room temperature after which they were subjected to further analysis. A pure PLA reference is processed following the same protocol. GPC analysis was conducted on all extruded samples to identify whether PLA degradation occurred in the presence of the various OBOCs (Supporting Information).

2.2. Analysis methods

^{1}H NMR spectra were recorded with a Bruker Ultrashield 300 spectrometer (300 MHz magnetic field). NMR-samples were prepared by dissolving ca. 10 mg of sample in 0.5 ml deuterated dimethyl sulfoxide (DMSO). Spectra were referenced against tetramethylsilane (d-TMS).

Weight average molecular weight (M_w) and polydispersity (PDI) of PLA blends after processing were determined from gel permeation chromatography (GPC) on a PSS SECcurity GPC system using Agilent 1260 Infinity instrument technology. The GPC system is equipped with two PFG combination medium micro-columns with 7 μm particle size (4.6 × 250 mm, separation range 100–1.000.000 Da), a PFG combination medium pre-column with 7 μm particle size (4.6 × 30 mm), and a Refractive Index detector (RI). Distilled 1,1,1,3,3,3-hexafluoroisopropanol (HFIP) containing 0.019% sodium trifluoroacetate was used as mobile phase at 40 °C, with a 0.3 mL/min flow rate. The GPC apparatus was calibrated with poly (methyl methacrylate) standards obtained from PSS. GPC samples were prepared by dissolving 5 mg of PLA in 1.5 ml HFIP overnight under constant shaking, the samples were filtered over a 0.2 μm PTFE syringe filter prior to injection.

The thermal behavior and transitions of the samples were identified via differential scanning calorimetry using a TA Instruments Q2000 DSC. All samples were measured at heating rate of 10 °C to a maximum temperature of 190 °C, kept isothermal for 3 min, and cooled back to room temperature at a rate of 1,3, 10, 30, or 100 °C/min unless mentioned otherwise. The glass transition temperature (T_g) and peak melting temperature (T_m) were determined from heating runs. The crystallization exotherm observed during the first cooling run was used to define peak crystallization temperature (T_c) and onset of crystallization temperature (T_{ons}). The peak crystallization temperature is considered the peak value of the crystallization exotherm, whereas the intersection of the tangents of the baseline and the crystallization curve is considered the onset temperature for crystallization. For isothermal crystallization, all samples are heated from room temperature to 190 °C at a rate of 10 °C/min and kept isothermal for 3 min to erase the thermal history. Next, these samples are cooled at a rate of 50 °C/min to the desired isothermal holding temperature (between 145 and 170 °C) to

allow nucleation and crystallization of the dissolved OXA molecules. After a 5 min isotherm at the holding temperature, the samples were cooled at a rate of 50 °C/min to 140 °C after which the isothermal crystallization of the PLA was monitored for 1 h. Reference samples were measured without subjection to an isothermal holding temperature, *i.e.* they were directly cooled to 140 °C at a rate of 50 °C/min after which the isothermal crystallization of the PLA was monitored. The obtained crystallization isotherms were subjected to an Avrami analysis [29]; The enthalpy of crystallization exotherm as a function of the isothermal time ($\Delta H_{(t)}$ in J/g) was divided over the total of the crystallization enthalpy (ΔH_{total} in J/g) to yield the crystalline mass fraction W_c. Note, the crystallization time was taken as $t - t_0$ where t_0 denotes that starting time of the crystallization exotherm. Next, the crystalline mass fraction was converted to the crystalline volume fraction (V_c), using equation (1),

$$V_c = \frac{W_c}{W_c + \left(\frac{\rho_c}{\rho_a}\right)(1 - W_c)} \quad (1)$$

where the ρ_c and ρ_a are the crystalline and amorphous densities of PLA, being 1.267 g/cm^3 and 1.257 g/cm^3, respectively [30].The Avrami parameters n (dimensionless) and k (in min^{-n}) can be extracted from the Avrami equation (2) after applying logarithmic properties to both sides, equation (3) [31],

$$1 - V_c = \exp(-kt^n) \quad (2)$$

$$Log[-\ln[1 - V_c(t)]] = Log(k) + n\log(t) \quad (3)$$

Classically, the Avrami parameter n is the summation of two terms, n_d and n_n, where n_d reflects the dimensionality of the growting crystals (1, 2, or 3), and n_n reflects the nucleation dependency which should vary between 0 (instantaneous nucleation) and 1 (sporadic nucleation) [31].

The morphological development during crystallization of the samples was monitored using polarized optical microscopy on an Olympus BX53 microscope mounted with an Olympus DP26 camera and a Linkam hotstage (between cross-polarizers and using a 530 nm λ-wave plate). The samples were heated to the desired temperature (generally 200 °C) at a rate of 30 °C/min. After leaving the samples for 3 min under isothermal conditions, the samples were cooled at a specified cooling rate (generally being 3, 10, or 30 °C/min) to the desired temperature where isothermal crystallization was monitored for 30 min. Optical micrographs depicting the morphological changes were recorded both during cooling and under isothermal conditions.

The evolution of the storage modulus of the PLA blends was followed over time at 200 °C in an Anton Paar 702 twin drive rheometer. A parallel plate geometry, having a diameter of 15 mm and gap of 750 μm, was used to study the time dependence of the storage modulus over temperature range from 200 °C to 80 °C. The strain (1%) and angular frequency (10 rad/s) were chosen such that the experiments were performed in the linear viscoelastic regime.

3. Results and discussion

3.1. OBOC as melt-miscible nucleating agent for PLA

The OBOCs synthesized in this study (Scheme 1) are designed such that they dissolve in the PLA melt at elevated temperatures and crystallize upon cooling. To ensure the interaction required for dissolution in PLA at elevated temperatures, the OBOCs contain two β-alanine ethyl ester end-groups, which are expected to exhibit a high affinity towards the PLA chains due to their structural similarity. Secondly, the introduction of the hydrogen bonding oxalamide motifs provides the driving force to crystallize during cooling. These two features, *i.e.* dissolution and crystallization of the OBOCs are clearly observed in optical microscopy: An example of the capability of the synthesized OBOCs to enhance the nucleation process for PLA is provided in Fig. 1, where the crystallization process of PLA in the presence of 2.0 wt% OXA4 is visualized during cooling. As expected, the OXA4 dissolves in the PLA melt, as a homogeneous mixture is obtained above the melting temperature of the PLA crystals. The crystallization of OXA4 molecules into branched crystals is detected around 138–136 °C during cooling at a rate of 10 °C/min, whereas the growth of the PLA crystals on the surface of the OXA4 crystals is immediately observed upon further cooling. Interestingly, we observe the development of a transcrystalline PLA morphology growing from the surface of the OXA4 crystals instead of spherulitic growth, indicated by the matching of the colors of the OXA4 crystals and the PLA crystals growing on their surface. Overall, this example clearly demonstrates that OXA4 crystals can effectively enhance the nucleation process of PLA, as the pure PLA sample does not display any notable crystallization when subjected to the same experimental protocol (Figure S12). The nucleating efficiency of the remaining OXA compounds as well as the main factors that govern it are detailed in the section below.

3.2. Effect of the OBOC crystallization temperature on transcrystalline PLA morphology

Strikingly different results are obtained when the same experimental protocol is followed for PLA containing 2.0 wt% OXA2 (Fig. 2). In contrast to OXA4, Fig. 2 reveals that the OXA2 crystal growth proceeds already at 174 °C during cooling at a rate of 10 °C/min and that the OXA2 crystals grow into relatively large needle shaped crystals instead of branched crystals. More importantly and in stark contrast to the 2.0 wt% OXA4 system, further cooling of the PLA sample containing 2.0 wt % OXA2 only results in the formation of a low number of PLA spherulites at 130 °C. The absence of the previously observed transcrystalline PLA morphology suggests that the OXA2 is a poor nucleating agent under the chosen experimental conditions. In contrast, when the OXA2 concentration is decreased to 1.0 wt%, OXA2 crystallization is observed at considerably lower temperatures of 143 °C (Fig. 3), which is immediately followed by the formation of a transcrystalline PLA morphology developing from the OXA2 crystal surface. These findings indicate that the nucleating efficiency of PLA in the presence of OXA2 increases when the crystallization temperature of the OXA2 molecules from the PLA melt decreases. Similarly, when subjecting PLA containing 2.0 wt% OXA6 to the same experimental protocol, OXA6 crystallization is observed at 132 °C, immediately followed by a transcrystalline PLA morphology developing from the OXA6 crystal surface (Figure S13). Overall, these findings support the notion that the PLA nucleating efficiency by the OBOCs is strongly dependent on the crystallization temperature of the OBOC molecules from the PLA melt, hence on the supersaturation of the OBOC solution upon crystallization.

In order to identify the interplay between the employed OBOC concentration and the melting temperature of the pure OBOC compounds, we have compiled a phase diagram depicting the dependency of the OBOC crystallization temperature from the PLA melt as a function of OBOC concentration (Fig. 4). Interestingly, no crystallization of the OXA3 and OXA5 was observed from the PLA melt upon cooling, likely originating from the low melting temperatures of the compounds (187 °C and 155 °C, respectively, Figure S6) and their relatively poor purity (Supporting information). For this reason, we will not focus on the behavior of OXA3 and OXA5 in this work and instead provide the relevant information of these samples in the Supporting Information. Accordingly, Fig. 4 only reflects systems containing OXA2, OXA4, and OXA6. In general, we observe that the OBOC crystallization temperature from the PLA melt decreases with decreasing concentration. Furthermore, as expected for miscible systems displaying a melting and crystallization temperature suppression, the phase diagram shows that the crystallization temperature follows the order OXA2 > OXA4 > OXA6 for a given OBOC concentration. Note that no OBOC crystallization was observed from the PLA in melt samples containing ≤0.5 wt% OXA2 and ≤1.0 wt% OXA4 or OXA6. We expect that the OBOC crystallization from

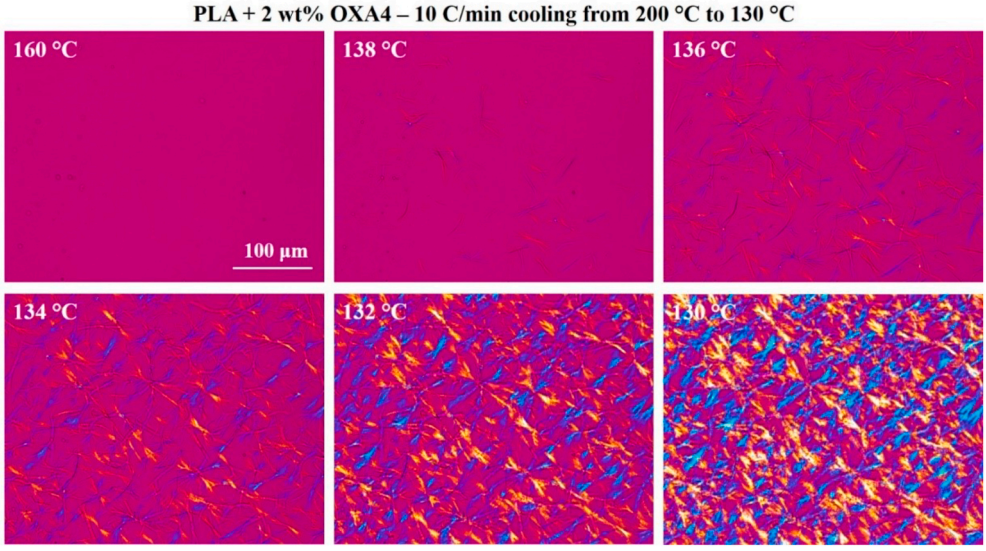

Fig. 1. Polarization optical micrographs depicting the morphological changes when cooling the sample containing PLA and 2.0 wt% OXA4 from 200 °C to 130 °C at a rate of 10 °C/min.

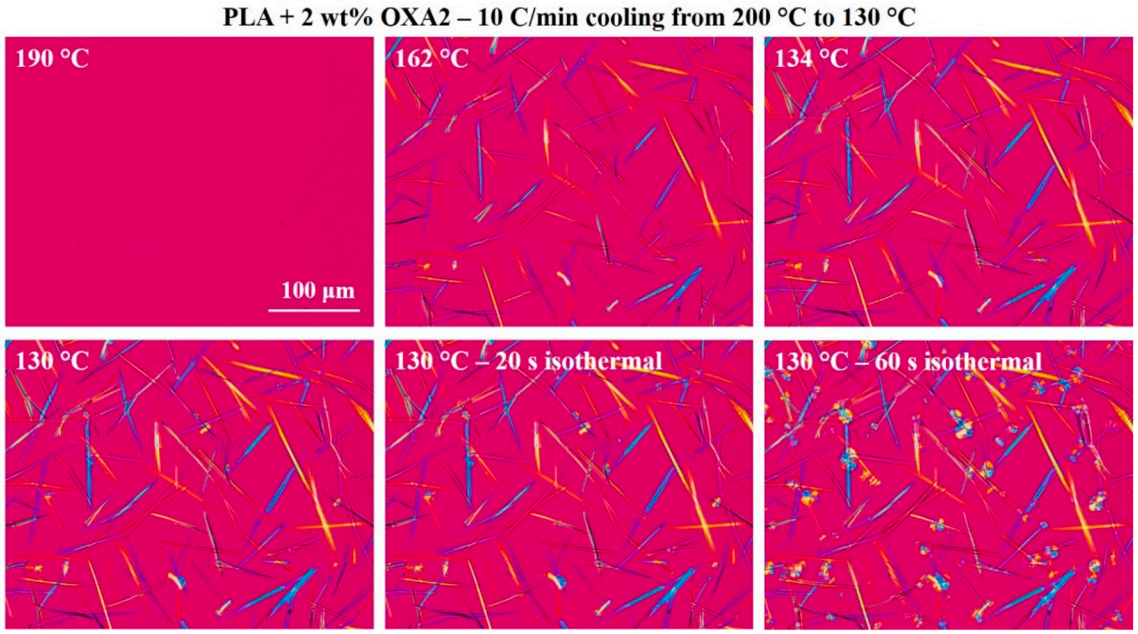

Fig. 2. Polarization optical micrographs depicting the morphological changes when cooling the sample containing PLA and 2.0 wt% OXA2 from 200 °C to 130 °C at a rate of 10 °C/min. Upon reaching 130 °C, the sample was kept isothermal for 1 min while the changes in optical morphology were monitored.

the PLA melt at such low concentrations proceeds only after crystallization of the PLA has occurred, and hence it is not observed under the chosen experimental conditions. The circled area denotes the combinations of OBOC concentrations and crystallization temperatures where a transcrystalline PLA morphology develops on the OBOC crystals surface during cooling. Overall, Fig. 4 shows that the enhancement in nucleating efficiency of PLA, indicated by the presence of a transcrystalline morphology, proceeds when the OBOC crystallizes around or below 145 °C. Systems for which OBOC crystallization sets off at higher temperatures do not exhibit such a significant enhancement in PLA nucleating efficiency, and the growth of spherulites, similar to those displayed in Fig. 2, is observed instead.

The aforementioned findings from polarized optical microscopy correspond well with findings from DSC. As can be observed from Fig. 5, left, no notable increase in peak crystallization temperature (T_c) of PLA is observed for the PLA containing 0.5 wt% OXA2 (T_c of 100 °C, compared to 99 °C for the pure PLA sample). As observed earlier, this directly relates to the inability of the OXA2 to crystallize from the PLA melt under these conditions, resulting in the homogeneous nucleation of PLA. As expected from Fig. 3, a significant increase in T_c to 115 °C is observed in the PLA containing 1.0 wt% OXA2. Similarly, when increasing the OXA2 concentration further, the T_c of PLA is observed at 102 (1.5 wt% OXA2) and 101 °C (2.0 wt% OXA2), undoubtedly resulting from the fact the OXA2 crystal were generated at too high temperatures. In addition, as is evident from Fig. 2, the generation of the OXA crystals in systems containing 1.5 and 2.0 wt% OXA2 results in a relatively poor dispersion of large OXA2 particles with a decreased surface-to-volume ratio (as is evident when comparing Figs. 2 and 3), inevitably decreasing the number of potential heterogeneous nucleation sites further.

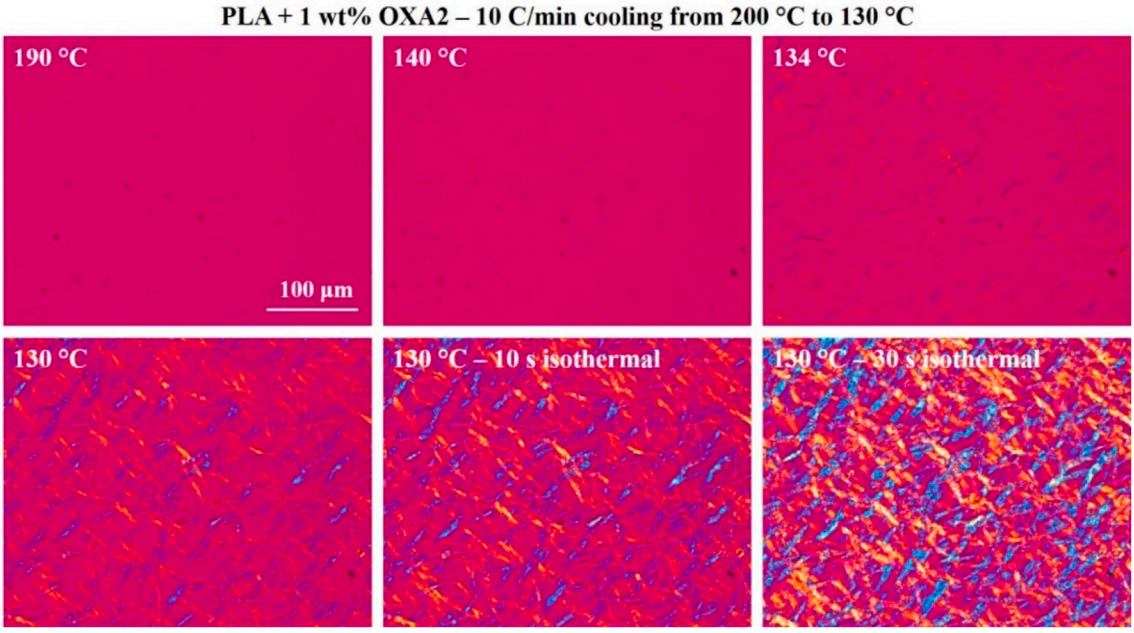

Fig. 3. Polarization optical micrographs depicting the morphological changes when cooling the sample containing PLA and 1.0 wt% OXA2 from 200 °C to 130 °C at a rate of 10 °C/min. Upon reaching 130 °C, the sample was kept isothermal for 1 min while the changes in optical morphology were monitored.

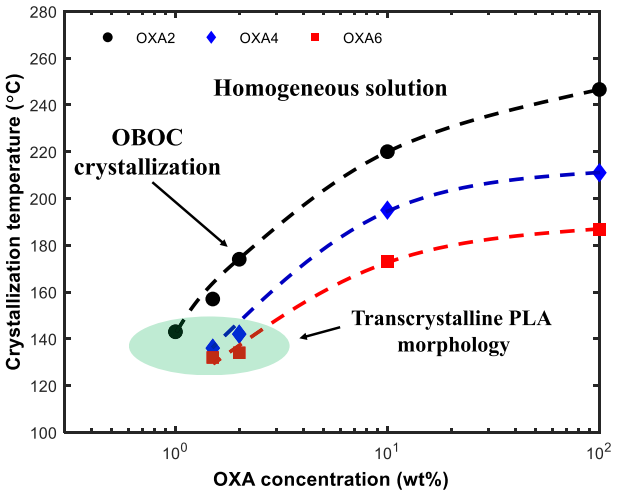

Fig. 4. Phase diagram depicting the crystallization temperature of OXA2, OXA4, and OXA6 from the PLA melt at various concentrations, as determined from polarized optical microscopy. The crystallization temperature reflects the visual observation of the OBOC crystals during cooling from the melt at a rate 10 °C/min. The region highlighted in green reflects the concentration range where a transcrystalline PLA morphology is observed on the OBOC crystal surface upon continued cooling. Note, the dotted lines are added to guide the eye of the reader. (For interpretation of the references to color in this figure legend, the reader is referred to the Web version of this article.)

The aforementioned trends are also observed in rheology (Fig. 5, right). Note that, when PLA samples containing OXA2 are cooled from the melt, the sudden deviation from Arrhenius type of behavior (pure PLA, Fig. 5 right) can be identified as the onset of PLA crystallization (T_{ons}). The sample containing 1.0 wt% OXA2 shows the highest T_{ons} of 125 °C, while the T_{ons} decreases in the samples containing 1.5 and 2.0 wt % OXA2 to 123 and 122 °C, respectively. More importantly, one can observe that the slope of the storage modulus during cooling to temperatures below T_{ons} is lower for samples containing 1.5 and 2.0 wt% OXA2, suggesting a slower increase in crystalline fraction, hence these systems contain a lower number of growing PLA crystals. As mentioned earlier, this is likely the result from the poorer OXA2 distribution, its lowered surface-to-volume ratio and the fact that the OXA2 crystals were grown at too high temperatures. It should be noted that there appears a discrepancy between the temperatures at which crystallization of the PLA phase is picked up in DSC and rheology methods; DSC monitors the release of energy resulting from the crystallization process, which might not be sensitive enough to detect the early stage of crystallization. In contrast, the visco-elastic response of polymer melts are highly sensitive to morphological changes and, as a result, rheology is able to pick up the presence of particles (*i.e.* growing crystals or fillers) having dimensions in the nanometer length scale. Accordingly, the crystallization process picked in the right image of Fig. 5 reflects the onset of the crystallization process whereas the information depicted in the left image of Fig. 5 represents an advanced stage of the crystallization process. The difference in crystallization, as observed from the different analysis techniques between the samples containing 1.5 and 2.0 wt% OXA2, is attributed to the poor nucleation ability of the OXA2 crystals grown under these experimental conditions. To clarify, the OXA2 crystals (at a concentration of 2.0 wt%) grown at a cooling rate of 10 °C/min, display a poor nucleating ability (Fig. 2), resulting in the growth of only a low number heterogeneous nuclei during cooling. While rheology picks up the presence and growth of these crystals, indicated by the increase in storage modulus, the overall crystal fraction (and accordingly, the released energy) remains very small and is only picked up as a deviation from baseline in DSC analysis (left image of Fig. 5). Due to lack of suitable OXA2 crystal surface for heterogeneous nucleation, the bulk PLA phase will undergo homogeneous nucleation during further cooling instead. Accordingly, a large increase in the volumetric crystalline component is only observed at temperatures comparable to that the pure PLA sample. In contrast, the PLA phase crystallizes rapidly upon extensive heterogeneous nucleation in the sample containing 1.0 wt% OXA2 (Fig. 3), which translates to a rapid increase in volumetric crystal fraction, and hence, a upwards shift in the crystallization peak in DSC analysis.

The attentive reader would argue that rheology is thereby able to pick up the OBOC crystallization process itself; Indeed, this is the case for the sample containing 2.0 wt% OXA2 as the crystallization of the OXA2 can be detected by the step-wise increase of the storage modulus around 160 °C. The absence of such a step-wise increase in storage

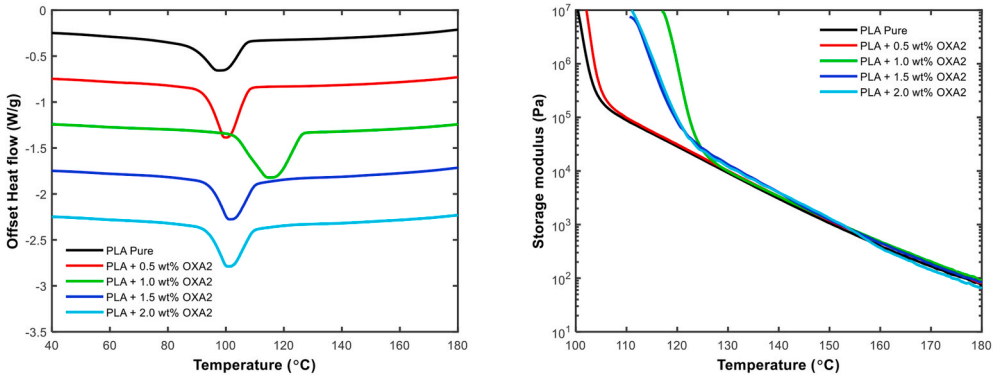

Fig. 5. Left, first DSC cooling traces taken at a cooling rate of 10 °C/min for systems having varying concentration of OXA2, depicting the characteristic crystallization exotherms. Right, the evaluation of the storage modulus observed during cooling at a rate of 5 °C/min for systems having varying OXA2 concentration.

modulus in systems containing OXA2 at lowered concentrations, however, is likely related to the size of the OXA2 crystals; in recent work we have demonstrated that the influence of the OBOC crystals on the visco-elastic behavior of *i*PP is strongly dependent on the OBOC crystallization conditions as changes in visco-elastic behavior are only observed for OBOC crystals having a critical size. We would like to refer the interested reader to consult previous work for detailed information on the OBOC influence on the visco-elastic behavior of polymer melts [25,52]. Lastly, the DSC and rheology data for the PLA samples with varying concentrations of the other OBOCs evaluated in this study are provided in the Supporting Information. Overall, these findings confirm that the capability of the OBOCs to enhance the nucleation efficiency of PLA is highest when the OBOC crystallizes around 145 °C or lower during cooling, irrespective of the chemical composition and the used OBOC concentration.

3.3. Identifying the OBOC nucleation mechanism

To obtain more information on the nucleation mechanism, we have performed the following experiment in polarized optical microscopy (Fig. 6): First, the sample containing 2.0 wt% OXA4 was heated to 200 °C to melt both the OXA4 and PLA crystals and to obtain a homogenous solution. Next, the sample was cooled to 145 °C at a rate of 30 °C/min where it was kept under isothermal conditions for 1 min to seed a low number of OXA4 crystals. Subsequently, the sample was heated at a rate of 30 °C/min to 155 °C and maintained at this temperature for 10 min to stimulate the growth of the OXA4 crystals. Interestingly, at 155 °C the growth of a few PLA spherulites is observed on the center of the OXA4 crystals, likely corresponding to the growth of crystals that nucleated during the isotherm at 145 °C (micrographs B and C, Fig. 6). After the 10 min isotherm at 155 °C, the sample is cooled at a rate of 10 °C/min to 130 °C, during which we observe 1) the further growth of existing OXA4 crystals, 2) the nucleation and growth of new OXA4 crystals, and 3) the nucleation and growth of PLA crystals. Interestingly, as is visible from the micrographs taken at 134 °C and 130 °C (micrographs E and F, Fig. 6), the formation of the transcrystalline PLA morphology is only observed on the 'freshly grown' OXA4 crystals parts; No PLA crystal growth is observed on the surface of the OXA4 crystals that were allowed to develop at 155 °C (examples highlighted in micrograph F, Fig. 6). Such behavior makes the possibility for either epitaxy or soft-epitaxy as nucleation mechanisms by the OXA4 crystals highly unlikely. If these were the nucleating mechanisms, one would anticipate the nucleating efficiency to be solely dependent on the surface-to-volume ratio and the dispersion of the OBOC crystals, and independent on the temperature at which they were generated.

Instead, we would like to consider both local stresses imposed on the PLA melt by the growing OBOC crystals and their surface roughness as two alternative parameters that affect the PLA nucleation process. The concept of stress-enhanced nucleation has already been suggested as nucleation mechanism for the formation of the transcrystalline crystallization morphology in fiber reinforced thermoplastic polymers, where stress build-up occurs during cooling as a result of the mismatch in thermal expansion coefficient of the fiber and material matrix [32–35]. In turn, the stresses imposed on the polymer melt can orient the contour of the polymer chains, a feature that is well known to lower the entropy of the chains and, hence, lower the nucleation barrier [36–38]. In our case, the growth of the OXA4 crystals will exert local stresses on the PLA melt in a similar manner, effectively imposing local shear on the PLA chains. The possibility for contour orientation, and hence stress-enhanced nucleation, can be evaluated by identification of the

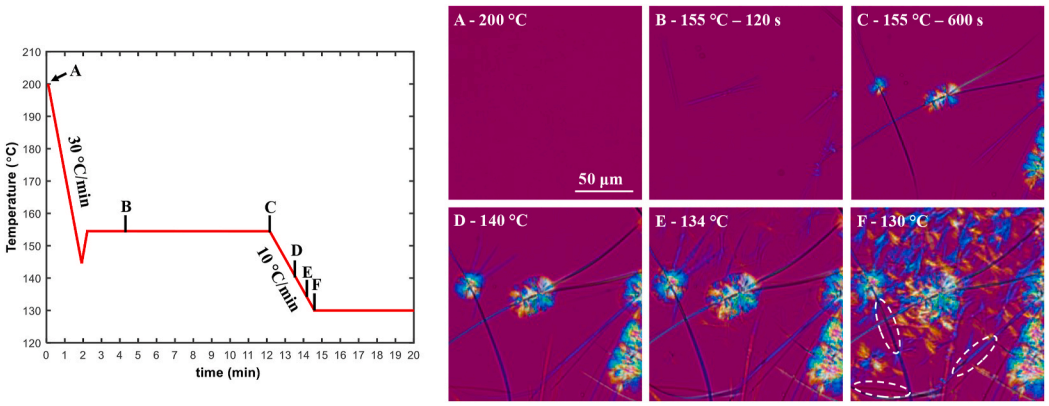

Fig. 6. Left, Experimental protocol used to identify the effect of OXA4 crystallization temperature on the PLA nucleation process. Right, polarization optical micrographs depicting the morphological changes, according to the letters displayed in the experimental protocol.

Weissenberg (*Wi*) number of this process. The dimensionless reptation or orientation *Wi* number is obtained by multiplying the imposed shear rate $\dot{\gamma}$ by the reptation time τ_{rep} and denotes the possibility for contour orientation of PLA chains when the value exceeds unity. In our experimental set-up, the local shear rate $\dot{\gamma}$ imposed on the PLA chains is approximated by taking the ratio of OXA4 crystal growth rate and the OXA4 radius at a given temperature or time. [39], whereas the reptation time τ_{rep} is obtained from rheology in combination with molecular modelling. The calculations used to determine both parameters are provided in detail in the Supporting Information. Notice that the Rouse Weissenberg numbers were estimated as well, though they are considerably lower than unity suggesting that rouse stretch is not realized under the experimental conditions of the current study. Instead, according to the calculations presented in the Supporting Information, during isothermal OXA4 crystallization at 140 °C, we observe that the growing OXA4 crystals can facilitate local shear rates of 0.6–1.2 s^{-1} on the PLA melt. This corresponds to W_i numbers for contour orientation of PLA chains between 0.3 and 0.6 (considering the whole molecular weight distribution) up to 1.8–3.6 (considering the 15% highest molecular weight chains). In other words, this approximation suggests that in particular the contour of the high molecular weight PLA chains orients by the shear rates imposed by the growing OXA4 crystals. Furthermore, these findings suggest that stress-enhanced nucleation is possible under the experimental conditions in this study.

To reflect, Iqbal and coworkers demonstrated in a recent study that shear-enhanced nucleation indeed proceeds when exposing the PLA to shear rates as low as 0.1 s^{-1} for 10 s at 140 °C [40]. However, though an enhancement in nucleation rate was observed compared to the pure PLA reference, Iqbal and coworkers observed an induction time of several minutes before crystallization proceeds after the application of the shear pulse. Furthermore, increasing the shear rate to $\dot{\gamma} = 2.0\ s^{-1}$ (10 s pulse) still resulted in an induction time of more than 100 s before crystallization was observed. Based on these findings, despite the continuous increase in both OXA4 crystal length and diameter, which effectively imposes a continuous stress on the PLA chains close to the growing OXA4 crystals, we would expect longer induction times for PLA nucleation and crystal growth than those observed in our experiments.

In addition, surface roughness, a parameter that is widely considered to influence the heterogeneous nucleation process. [41–46], is likely to enhance the nucleation process of PLA in the presence of the growing OXA4 crystal even further. The argumentation is as follows: Freshly grown OXA4 crystal parts are likely to contain defects such as dislocations, potentially generating crystals with a high surface roughness. Following the findings depicted in Fig. 2, the OXA4 crystals grown at 155 °C do not facilitate heterogeneous nucleation of the PLA matrix, indicating that they might contain less defects and hence a lowered surface roughness. The origin of this difference in surface roughness can be two-fold. First, the 'freshly grown' OXA4 crystal segments contain a high number of defects, which reorganize and/or recrystallize during the isothermal annealing step at 155 °C. Second, we consider it likely that crystals formed at elevated temperatures are already less defected resulting from the lower supersaturation of the system, which decreases both the crystal growth rate and the chance of defect formation. Either way, the OXA4 crystals generated at or exposed to elevated temperatures are expected to exhibit low surface roughness, decreasing their capability to promote heterogeneous nucleation of PLA.

To verify these findings from polarized optical microscopy and support the above mentioned hypotheses, isothermal crystallization studies were performed and subjected to an Avrami analysis [29,31]. To this end, PLA samples with and without 2.0 wt% OXA2 were heated to 190 °C and kept isothermal for 3 min to ensure both the PLA and the OXA2 are molten and to erase the thermal history of the sample. The sample was cooled at a rate of 50 °C/min to a first isothermal (holding) temperature between 145 and 170 °C for 5 min to allow for the generation of OXA2 crystals. Next, the sample was cooled at a rate of 50 °C/min to 140 °C after which the isothermal crystallization of the PLA was monitored (Fig. 7A). As reference, the isothermal crystallization for both pure PLA and PLA with 2.0 wt% OXA2 was monitored after cooling to 140 °C directly (black and red lines in Fig. 7, respectively). The isothermal crystallization exotherms displayed in Fig. 7B clearly demonstrate that the PLA reference (black line) crystallizes particularly slowly at 140 °C, with a half-time of crystallization (t_{half}-t_0) of 26.5 min. In contrast, the presence of 2.0 wt% OXA2 decreases t_{half}-t_0 significantly to 4.0 when subjecting the sample to the same experimental protocol (red line, Fig. 7B).

Unfortunately, the samples subjected to a holding temperature of 145 °C and 150 °C started to crystallize already at the holding temperature, preventing us from obtaining a useable crystallization exotherm upon cooling to 140 °C and are therefore excluded from further analysis. However, as expected, the isothermal crystallization process of PLA with 2.0 wt% OXA2 at 140 °C is slowed down for samples which were subjected to a first isothermal temperature between 155 °C and 160 °C (t_{half}-t_0 of 8.5 and 8.6 min, respectively). As can be deduced from Fig. 6, only a part of the dissolved OXA2 molecules is taken up in the OXA2 crystals growing during the isothermal holding temperature, yielding crystals that are unable to promote heterogeneous nucleation upon further cooling to 140 °C. Instead, the enhancement in nucleation efficiency compared to the pure PLA sample originates from the remainder of the dissolved OXA2 molecules that crystallize during/after cooling to 140 °C and effectively facilitate the growth of a transcrystalline morphology. However, a lower number of heterogeneous nucleation events can be expected as a result of the presence of 'inert' OXA2 crystals (*i.e.* without the ability to facilitate heterogeneous nucleation of PLA crystals), translating into a slower increase of the volumetric crystalline fraction (V_c) over time when compared to the same sample immediately cooled to 140 °C (Fig. 7C). This effect diminishes for samples subjected to an isothermal holding temperature of 165 or 170 °C (t_{half}-t_0 of 5.2 and 4.1 min, respectively), as the rate of OXA2 crystallization at this holding temperature is very low. Accordingly, a high OXA2 concentration remains dissolved at the holding temperature and only crystallizes during cooling to or upon reaching 140 °C, effectively yielding a scenario very similar to the system which was directly cooled to 140 °C.

The difference in nucleation density in the different systems becomes evident when comparing the Avrami plots of the different samples (Fig. 7D). For example, for the pure PLA reference (black line) we observe n = 2.75, a value significantly larger than for the PLA with 2.0 wt% OXA2 reference (red line), which yields n = 2.03. Classically, an Avrami parameter n of 2 would suggest the growth of 2-dimensional crystals and the occurrence of instantaneous nucleation [31], two features which can be expected in the presence of OXA2 crystals as they stimulate transcrystalline PLA crystal growth under the right conditions (Fig. 3). The value of n = 2.75 for the pure PLA reference is close to the values reported in literature (varying from 2.4 to 3.3) [30,47] and is generally attributed to athermal and three-dimensional crystal growth. When subjecting the PLA with 2.0 wt% OXA2 to an isothermal holding time at 155 °C or 160 °C prior to isothermal crystallization at 140 °C, the Avrami parameter n slowly increases to 2.24 and 2.40, respectively, suggesting a decrease in nucleation rate and/or a change in PLA crystal morphology. As explained above, such a change in nucleation and crystallization behavior is expected as part of the OXA2 is depleted during the isothermal holding temperature and is unable to facilitate heterogeneous nucleation of the PLA upon consecutive cooling. As expected, when increasing the holding temperature further, the Avrami parameter n decreases again to 2.11 and 2.27 (holding temperatures of 165 °C and 170 °C, respectively). We would like to highlight that one should consider the obtained Avrami parameters as qualitative given that the nucleation and crystallization processes in these samples are rather complex combined with the fact that crystallization proceeds in some samples already during cooling towards 140 °C (Fig. 7B). Nevertheless, these findings depict a clear trend in crystallization behavior that supports the observation that OXA crystals grown at elevated temperatures are unable to provide surface for heterogeneous

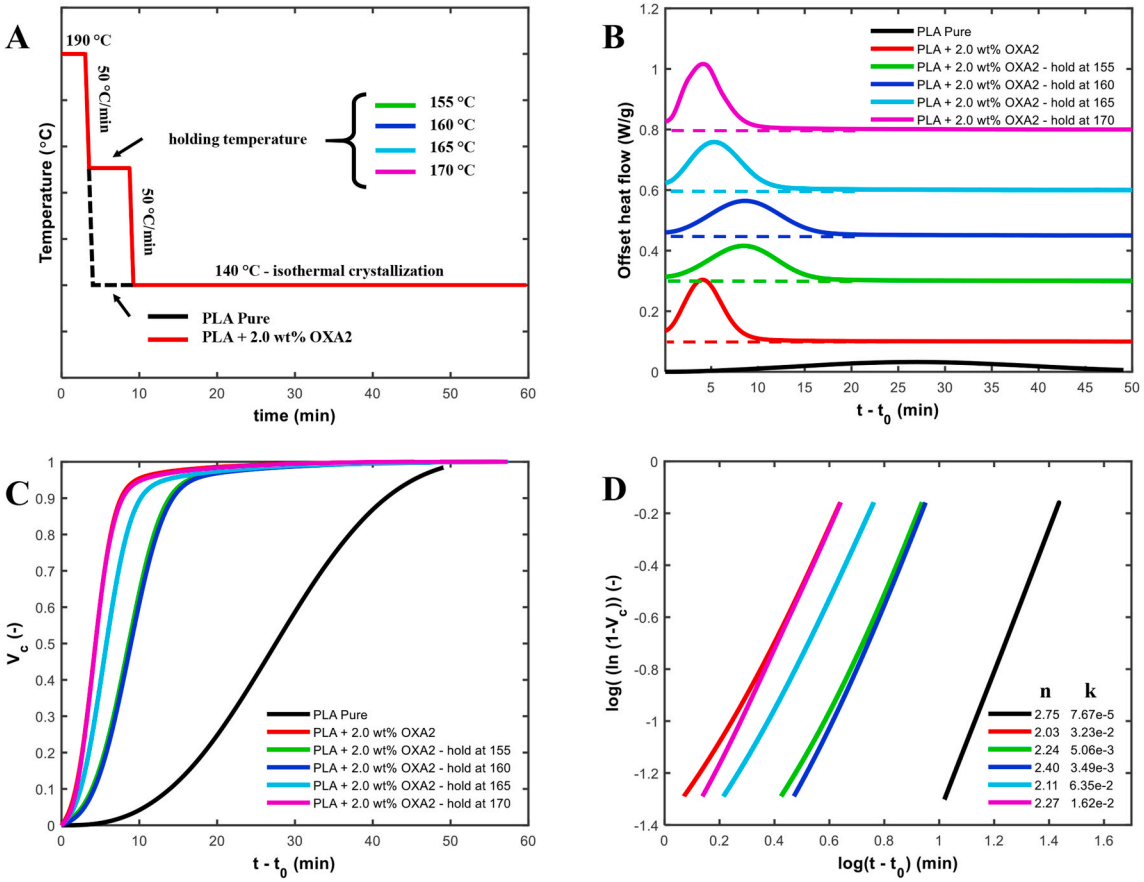

Fig. 7. A) Schematic overview of experimental protocol employed to assess the effect the influence of OXA2 crystallization temperature on the isothermal crystallization of PLA at 140 °C. B) Isothermal crystallization isotherms (exo up) obtained at 140 °C following the experimental protocol displayed in image A). C) Development of the relative volumetric crystalline fraction (V_c) during isotherml crystallization at 140 °C. D) Overview of Avrami plots taking into account the development of V_c between 5 and 50% (k in min^{-n}).

nucleation of PLA, and hence, result in a decrease in nucleating efficiency of this class of nucleating agents.

3.4. Optimizing processing conditions for improved PLA nucleation

Retrospectively, we learned that the OBOC crystal growth should proceed at temperatures around 150-145 °C or lower for the formation of a transcrystalline PLA morphology on the OBOC crystal surface. The critical parameter that drives the OBOC nucleation and crystal growth rate is the supersaturation, which is governed by the pure OBOC melting temperature, the employed OBOC concentration, and the imposed cooling rate [48–51]. In the previous section, we have elaborated on the interplay between the OBOC melting temperature, concentration, and thermal history on the PLA crystallization morphology (Fig. 4), leaving the cooling rate as an additional parameter. When subjecting the samples to increasing cooling rates, a higher supersaturation can be achieved before the OBOC crystallization proceeds from the PLA melt. As both the OBOC nucleation and growth rate are generally expected to increase with increasing supersaturation [48], the OBOC will crystallize with an increasing surface-to-volume ratio, hence there will be more surface available for heterogeneous nucleation of PLA [24,25]. In addition, increased OBOC growth rates will increase both the local stresses imposed on the PLA melt and the defects and surface roughness of the generated OBOC crystals. For example, as described in the previous sections, during cooling at a rate of 10 °C/min, the OXA2 is not effective in generating a transcrystalline PLA morphology when used in a concentration of 2.0 wt%, while the OXA4 and OXA6 systems are. However, when subjecting these same samples to a cooling rate of 50 °C/min, one can observe the OXA2 becomes the most efficient nucleating agent when monitoring the isothermal crystallization at 135 °C (Fig. 8, left). For example, the crystallization half-time (t_{half} - t_0) observed under these conditions is 2.7 min, 8.6 min and more than 30 min for the systems containing 2 wt% OXA2, OXA4, and OXA6 respectively. For comparison, pure PLA displays a t_{half} - t_0 of 17.7 min, indicating that the presence of 2.0 wt% OXA6 in fact delays the nucleation and crystallization process under these conditions. Such a delay in nucleation and crystallization rate is a characteristic feature of a plasticizer; Indeed, as observed from Figure S13, OXA6 remains dissolved at this temperature and could indeed act as a plasticizer, as we have reported for OBOCs dissolved in isotactic polypropylene [24,52].

When performing the same isothermal crystallization experiments for the PLA containing 2.0 wt% OXA2, but at different isothermal temperatures (Fig. 8, right) we observe that PLA crystallization proceeds rapidly at 145 °C and lower, in line with the previous findings. However, the crystallization half-time (t_{half} – t_0) increases rapidly during isothermal crystallization at 150 °C, suggesting that the OXA2 crystal growth proceeds sufficiently slow to 1) allow for the PLA phase to relax all imposed stresses and 2) develop crystals with a low surface roughness. Note, the decrease in PLA crystal growth rate as a function of the decreasing undercooling of the PLA melt should be taken into account. Nevertheless, the findings displayed in Figs. 7 and 8 confirm that a high cooling rate and the selection of a low crystallization temperature (≤145 °C) are essential for an optimal OBOC nucleation efficiency. These features are favorable for use under industrial processing conditions, as they generally require high cooling rates.

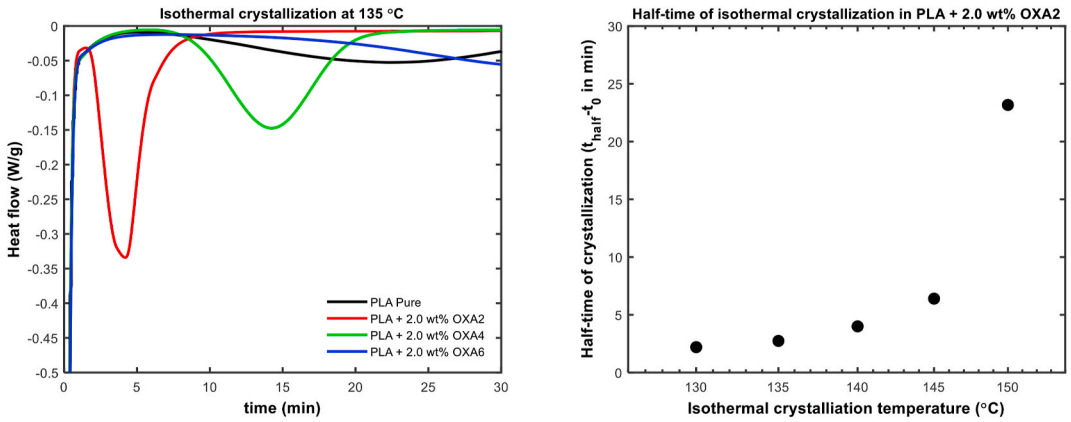

Fig. 8. Left, DSC thermograms depicting the crystallization exotherm observed during isothermal conditions (at 135 °C) after cooling pure PLA, and PLA with 2.0 wt % OXA2, OXA4, and OXA6 from the melt at a rate of 100 °C/min to 135 °C. Right, half-time of crystallization (t_{half} - t_0) as a function of the isothermal crystallization temperature in PLA systems containing 2.0 wt% OXA2, observed from DSC experiments after cooling from 200 °C to the desired isothermal crystallization temperature at a rate of 50 °C/min.

4. Conclusions

In this work, we synthesized five different melt-soluble oxalamide based organic compounds (OBOCs) and evaluated their nucleation mechanism for PLA. The OBOCs indeed dissolve at elevated temperatures in the PLA melt and, dependent on the pure OBOC melting temperature and the used concentration, crystallizes upon cooling after which they provide a surface for heterogeneous nucleation to PLA. However, the effective nucleation efficiency seems highly dependent on the crystallization temperature of the OBOC from the PLA melt. These findings indicate that epitaxy or soft-epitaxy are unlikely nucleation mechanisms for these OBOCs. Instead, we identify surface roughness of the OBOC crystals in combination with local stresses imposed on the PLA melt by the growing OBOC crystals as critical parameters to explain this variation in nucleation efficiency. Since both surface roughness and OBOC crystal growth rates increase with increasing supersaturation, the use of OBOCs as nucleating agents is identified to be more suitable in processes where high cooling rates are desired. In this respect, the role of OBOCs is rather unique compared to the reported nucleating agents for PLAs in the literature.

Declaration of competing interest

The authors declare that they have no known competing financial interests or personal relationships that could have appeared to influence the work reported in this paper.

CRediT authorship contribution statement

Manta Roy: Conceptualization, Methodology, Investigation, Writing - original draft. **Maksim Zhelezniakov:** Investigation. **Gijs W. de Kort:** Investigation. **Laurence G.D. Hawke:** Investigation. **Nils Leoné:** Investigation. **Sanjay Rastogi:** Supervision, Writing - review & editing. **Carolus H.R.M. Wilsens:** Conceptualization, Funding acquisition, Supervision, Writing - original draft, Writing - review & editing.

Acknowledgement

This project has received funding from the INTERREG V program Flanders-Netherlands (Puur Natuur: 100% Biobased), the cross-border collaboration program financially supported by the European fund for regional development.

Appendix A. Supplementary data

Supplementary data to this article can be found online at https://doi.org/10.1016/j.polymer.2020.122680.

Supporting Information

Additional information on synthesis of bisoxalamide based nucleating agents (Figure S1-S5) characteristic thermal behavior of OBOCs synthesized in this study (Figure S6), overview of GPC data of PLA after processing with various concentrations of OXA nucleating agents (Table S1), PLA crystallization in the absence of OBOC (Figure S7), crystallization morphology of PLA in the presence of 2.0 wt% OXA6 (Figure S8), identification of rouse relaxation time for PLA (Figure S9-S10), approximation of shear rates during OBOC crystal growth (Table S2, Figure S11-S14), PLA crystallization during cooling in the presence of OBOC in varying concentration (Figure S15-S16).

References

[1] S. Kwon, P.C. Lee, E.G. Lee, Y. Keun Chang, N. Chang, Production of lactic acid by lactobacillus rhamnosus with vitamin- supplemented soybean hydrolysate, Enzym. Microb. Technol. 26 (2–4) (2000) 209–215, https://doi.org/10.1016/S0141-0229(99)00134-9.

[2] C. Gao, C. Ma, P. Xu, Biotechnological routes based on lactic acid production from biomass, Biotechnol. Adv. 29 (6) (2011) 930–939, https://doi.org/10.1016/j.biotechadv.2011.07.022.

[3] D. Bilanovic, F.H. Chang, P. Isobaev, P. Welle, Lactic acid and xanthan fermentations on an alternative potato residues media - carbon source costs, Biomass Bioenergy 35 (7) (2011) 2683–2689, https://doi.org/10.1016/j.biombioe.2011.03.001.

[4] K. Fukushima, K. Sogo, S. Miura, Y. Kimura, Production of D -Lactic acid by bacterial fermentation of rice starch, Macromol. Biosci. (2004) 1021–1027, https://doi.org/10.1002/mabi.200400080.

[5] C.V. Leal, R. dos Santos Almeida, J.L. Dávila, J.A. Domingues, M.A. Hausen, E.A. R. Duek, M.A. d'Ávila, Characterization and in vitro evaluation of electrospun aligned-fiber membranes of poly(L-Co-D,L-Lactic acid), J. Appl. Polym. Sci. 47657 (2019) 1–9, https://doi.org/10.1002/app.47657.

[6] P.T. Bertuoli, J. Ordono, E. Armelin, S. Pérez-Amodio, A.F. Baldissera, C. A. Ferreira, J. Puiggalí, E. Engel, L.J. Del Valle, C. Alemán, Electrospun conducting and biocompatible uniaxial and core-shell fibers having poly(lactic acid), poly (ethylene glycol), and polyaniline for cardiac tissue engineering, ACS Omega 4 (2) (2019) 3660–3672, https://doi.org/10.1021/acsomega.8b03411.

[7] S. Frackowiak, J. Ludwiczak, K. Leluk, Man-made and natural fibres as a reinforcement in fully biodegradable polymer composites: a concise study, J. Polym. Environ. 26 (12) (2018) 4360–4368, https://doi.org/10.1007/s10924-018-1301-9.

[8] M. Morreale, M.C. Mistretta, V. Fiore, Creep behavior of poly(lactic acid) based biocomposites, Materials 10 (4) (2017), https://doi.org/10.3390/ma10040395.

[9] T. Tábi, P. Bakonyi, S. Hajba, P.J. Herrera-Franco, T. Czigány, J.G. Kovács, Creep behaviour of injection-moulded basalt fibre reinforced poly(lactic acid) composites, J. Reinforc. Plast. Compos. 35 (21) (2016) 1600–1610, https://doi.org/10.1177/0731684416661239.

[10] F. De Santis, V. Volpe, R. Pantani, Effect of molding conditions on crystallization kinetics and mechanical properties of poly (lactic acid), Polym. Eng. Sci. 1–6 (2017), https://doi.org/10.1002/pen.24414.
[11] J.Z. Xu, Z.J. Zhang, H. Xu, J. Bin Chen, R. Ran, Z.M. Li, Highly enhanced crystallization kinetics of poly(l -lactic acid) by poly(ethylene glycol) grafted graphene oxide simultaneously as heterogeneous nucleation agent and chain mobility promoter, Macromolecules 48 (14) (2015) 4891–4900, https://doi.org/10.1021/acs.macromol.5b00462.
[12] Q. Xie, L. Han, G. Shan, Y. Bao, P. Pan, Polymorphic Crystalline Structure and Crystal Morphology of Enantiomeric Poly(Lactic Acid) Blends Tailored by a Self-Assemblable Aryl Amide Nucleator, 2016, https://doi.org/10.1021/acssuschemeng.6b00191.
[13] H.Y. Yin, X.F. Wei, R.Y. Bao, Q.X. Dong, Z.Y. Liu, W. Yang, B.H. Xie, M.B. Yang, High-melting-point crystals of poly(l-lactic acid) (PLLA): the most efficient nucleating agent to enhance the crystallization of PLLA, CrystEngComm 17 (11) (2015) 2310–2320, https://doi.org/10.1039/c4ce02497d.
[14] J.Z. Liang, L. Zhou, C.Y. Tang, C.P. Tsui, Crystalline properties of poly(L-lactic acid) composites filled with nanometer calcium carbonate, Compos. B Eng. 45 (1) (2013) 1646–1650, https://doi.org/10.1016/j.compositesb.2012.09.086.
[15] Pei, A.; Zhou, Q.; Berglund, L. A. Functionalized cellulose nanocrystals as biobased nucleation agents in poly (L -lactide) (PLLA) crystallization and mechanical property effects. 2010, 70, 815–821. https://doi.org/10.1016/j.compscitech.2010.01.018.
[16] R. Neppalli, V. Causin, C. Marega, M. Modesti, R. Adhikari, S. Scholtyssek, S.S. Ray, A. Marigo, The effect of different clays on the structure, morphology and degradation behavior of poly(lactic acid), Appl. Clay Sci. 87 (2014) 278–284, https://doi.org/10.1016/j.clay.2013.11.029.
[17] F. De Santis, R. Pantani, Melt compounding of poly (lactic acid) and talc: assessment of material behavior during processing and resulting crystallization, J. Polym. Res. 22 (12) (2015) 1–9, https://doi.org/10.1007/s10965-015-0885-1.
[18] A. Gupta, W. Simmons, G.T. Schueneman, E.A. Mintz, Lignin-coated cellulose nanocrystals as promising nucleating agent for poly(lactic acid), J. Therm. Anal. Calorim. 126 (3) (2016) 1243–1251, https://doi.org/10.1007/s10973-016-5657-6.
[19] Y. Fan, J. Zhu, S. Yan, X. Chen, J. Yin, Nucleating effect and crystal morphology controlling based on binary phase behavior between organic nucleating agent and poly(l-lactic acid), Polymer 67 (2015) 63–71, https://doi.org/10.1016/j.polymer.2015.04.062.
[20] T. Xu, A. Zhang, Y. Zhao, Z. Han, L. Xue, Crystallization kinetics and morphology of biodegradable poly (lactic acid) with a hydrazide nucleating agent, Polym. Test. 45 (2015) 101–106, https://doi.org/10.1016/j.polymertesting.2015.05.009.
[21] M.J. Carbone, M. Vanhalle, B. Goderis, P. Van Puyvelde, Amino acids and poly (amino acids) as nucleating agents for poly(lactic acid), J. Polym. Eng. 35 (2) (2015) 169–180, https://doi.org/10.1515/polyeng-2014-0175.
[22] Y. Xu, D. Wang, W. Dong, M. Chen, Rapid crystallization of poly(lactic acid) by using tailor-made oxalamide derivatives as novel soluble-type nucleating agents, *Ind.* Eng. Chem. Res. 53 (32) (2014) 12888–12892, https://doi.org/10.1021/ie502211j.
[23] P. Ma, Y.S. Deshmukh, C.H.R.M. Wilsens, M. Ryan Hansen, R. Graf, S. Rastogi, Self-assembling process of oxalamide compounds and their nucleation efficiency in biodegradable poly(hydroxyalkanoate)s, Sci. Rep. 5 (February) (2015) 1–9, https://doi.org/10.1038/srep13280.
[24] C.H.R.M. Wilsens, L.G.D. Hawke, E.M. Troisi, D. Hermida-Merino, G. De Kort, N. Leoné, K. Saralidze, G.W.M. Peters, S. Rastogi, Effect of self-assembly of oxalamide based organic compounds on melt behavior, nucleation, and crystallization of isotactic polypropylene, Macromolecules 51 (13) (2018) 4882–4895, https://doi.org/10.1021/acs.macromol.8b00489.
[25] Y.S. Deshmukh, C.H.R.M. Wilsens, N. Leone, G. Portale, J.A.W. Harings, S. Rastogi, Melt-miscible oxalamide based nucleating agents and their nucleation efficiency in isotactic polypropylene, Ind. Eng. Chem. Res. 55 (45) (2016) 11756–11766, https://doi.org/10.1021/acs.iecr.6b03120.
[26] P. Ma, Y. Xu, T. Shen, W. Dong, M. Chen, P.J. Lemstra, Tailoring the crystallization behavior of poly(L-lactide) with self-assembly-type oxalamide compounds as nucleators: 1. Effect of terminal configuration of the nucleators, Eur. Polym. J. 70 (2015) 400–411, https://doi.org/10.1016/j.eurpolymj.2015.07.040.
[27] J. Yang, R. Liang, R. Kong, Y. Chen, X. Wang, J. Yin, J. Wan, X. Wang, C. Bi, Crystal morphology, crystallization behavior, polymorphic crystalline structure and thermal stability of poly(1,4-butylene adipate) modulated by a oxalamide derivative nucleating agent, Polym. Degrad. Stabil. 144 (2017) 33–42, https://doi.org/10.1016/j.polymdegradstab.2017.07.030.
[28] J. Yang, R. Liang, Y. Chen, C. Zhang, R. Zhang, X. Wang, R. Kong, Q. Chen, Using a self-assemblable nucleating agent to tailor crystallization behavior, crystal morphology, polymorphic crystalline structure, and biodegradability of poly(1,4-butylene adipate), Ind. Eng. Chem. Res. 56 (28) (2017) 7910–7919, https://doi.org/10.1021/acs.iecr.7b01783.
[29] M. Avrami, Kinetics of phase change. II transformation-time relations for random distribution of nuclei, J. Chem. Phys. 8 (1940) 212, https://doi.org/10.1063/1.1750631.
[30] T. Miyata, T. Masuko, Crystallization behavior of poly(l-lactide), Polymer 39 (22) (1998) 5515–5521, https://doi.org/10.1016/S0032-3861(97)10203-8.
[31] A.T. Lorenzo, M.L. Arnal, J. Albuerne, A.J. Muller, DSC isothermal polymer crystallization kinetics measurements and the use of the Avrami equation to fit the data: guidelines to avoid common problems, Polym. Test. 26 (2007) 222–231. https:// do.org/:10.1016/j.polymertesting.2006.10.005.
[32] J.L. Thomason, A.A. Van Rooyen, Transcrystallized interphase in thermoplastic composites, J. Mater. Sci. 27 (4) (1992) 897–907, https://doi.org/10.1007/BF01197639.
[33] D. Gray, "Transcrystallization" induced by mechanical stress on a polypropylene melt, J. Polym. Sci., Polym. Lett. Ed. 12 (11) (1974) 645–650, https://doi.org/10.1002/pol.1974.130121107.
[34] C. Wang, C.R. Liu, Transcrystallization of polypropylene on carbon fibres, Polymer 38 (18) (1997) 4715–4718, https://doi.org/10.1016/S0032-3861(96)01083-X.
[35] C. Wang, C.-R. Liu, Transcrystallization of polypropylene composites: nucleating ability of fibres, Polymer 40 (2) (1999) 289–298, https://doi.org/10.1016/S0032-3861(98)00240-7.
[36] J. Van Meerveld, G.W.M. Peters, M. Hütter, Towards a rheological classification of flow induced crystallization experiments of polymer melts, Rheol. Acta (2004) 119–134, https://doi.org/10.1007/s00397-004-0382-7.
[37] S. Acierno, B. Palomba, H. Henning Winter, N. Grizutti, Effect of molecular weight on the flow-induced crystallization of isotactic poly(1-butene), Rheol. Acta 42 (2003) 243–250, https://doi.org/10.1007/s00397-002-0280-9.
[38] S. Coppola, L. Balzano, E. Giofreddi, P.L. Maffetone, N. Grizutti, Effects of the degree of undercooling on flow induced crystallization in polymer melts, Polymer 45 (10) (2004) 3249–3256, https://doi.org/10.1016/j.polymer.2004.03.049.
[39] F. Ahonguio, L. Jossic, A. Magnin, Motion and stability of cones in a yield stress fluid, AIChE J. 61 (2015) 709–717, https://doi.org/10.1002/aic.14651.
[40] N. Iqbal, K. Jariyavidyanont, A.M. Rhoades, R. Androsch, Critical specific work of flow for shear-induced formation of crystal nuclei in poly (L-lactic acid), Polymer Crystallization (2019), e10073, https://doi.org/10.1002/pcr2.10073.
[41] P. Damman, S. Coppée, V.M. Geskin, R. Lazzaroni, What is the mechanism of oriented crystal growth on rubbed polymer substrates? Topography vs epitaxy, J. Am. Chem. Soc. 124 (51) (2002) 15166–15167, https://doi.org/10.1021/ja027145l.
[42] C. Lin, S. Ding, Y. Hwang, Interfacial crystallization of isotactic polypropylene molded against the copper surface with various surface roughnesses prepared by an electrochemical process, J. Mater. Sci. 36 (20) (2001) 4943–4948. https://link.springer.com/article/10.1023/A:1011848623699.
[43] A.J. Page, R.P. Sear, Crystallization controlled by the geometry of a surface, J. Am. Chem. Soc. 131 (48) (2009) 17550–17551, https://doi.org/10.1021/ja9085512.
[44] G. Di Profio, E. Fontananova, E. Curcio, E. Drioli, From tailored supports to controlled nucleation: exploring material chemistry, surface nanostructure, and wetting regime effects in heterogeneous nucleation of organic molecules, Cryst. Growth Des. 12 (7) (2012) 3749–3757, https://doi.org/10.1021/cg3005568.
[45] J. Holbrough, J. Campbell, F. Meldrum, H. Christenson, Topographical control of crystal nucleation, Cryst. Growth Des. 12 (2) (2012) 750–755, https://doi.org/10.1021/cg201084j.
[46] B. Wang, T. Wen, X. Zhang, A. Tercjak, X. Dong, A.J. Muller, D. Wang, D. Cavallo, Nucleation of poly(lactide) on the surface of different fibers, Macromolecules 52 (16) (2019) 6274–6284, https://doi.org/10.1021/acs.macromol.9b01078.
[47] P.J.A. Lohmeijer, J.P.A. Goossens, G.W.M. Peters, Quiescent crystallization of poly (lactic acid) studied by optical microscopy and light-scattering techniques, J. Appl. Polym. Sci. 44566 (2017) 1–9, https://doi.org/10.1002/APP.44566.
[48] R. Boistelle, J.P. Astier, Crystallization mechanism in solution, J. Cryst. Growth 40 (1988) 14–29, https://doi.org/10.1016/0022-0248(88)90294-1.
[49] V.A. Petrovsky, V.I. Rakin, Holographic studies of the solution surrounding a growing or dissolving crystal, J. Cryst. Growth 56 (1982) 7–14, https://doi.org/10.1016/0022-0248(82)90006-9.
[50] J. Garside, Industrial crystallization from solution, Chem. Eng. Sci. 40 (1984) 3–26, https://doi.org/10.1016/0009-2509(85)85043-0.
[51] N. Leoné, M. Roy, S. Saidi, G. de Kort, D. Hermida-Merino, C.H.R.M. Wilsens, Improving processing, crystallization, and performance of poly-l-lactide with an amide-based organic compound as both plasticizer and nucleating agent, ACS Omega 46 (2019) 10376–10387, https://doi.org/10.1021/acsomega.9b00848.
[52] C.H.R.M. Wilsens, L.G.D. Hawke, G.W. de Kort, S. Saidi, M. Roy, N. Leoné, D. Hermida-Merino, G.W.M. Peters, S. Rastogi, Effect of thermal history and shear on the viscoelastic response of iPP containing an oxalamide-based organic compound, Macromolecules 52 (7) (2019) 2789–2802, https://doi.org/10.1021/acs.macromol.8b02612.